Black Phosphorus Gas Sensors

Ahmad N. Abbas,[†,‡] Bilu Liu,[†] Liang Chen,[†] Yuqiang Ma,[†] Sen Cong,[†] Noppadol Aroonyadet,[†] Marianne Köpf,[§] Tom Nilges,[§] and Chongwu Zhou*[,†]

[†]Department of Electrical Engineering, University of Southern California, Los Angeles, California 90089, United States, [‡]Department of Electrical Engineering, University of Jeddah, Abdullah Sulayman Street, Jeddah 22254, Saudi Arabia, and [§]Department of Chemistry, Technische Universität München, Lichtenbergstraße 4, Garching b, München 485748, Germany

ABSTRACT The utilization of black phosphorus and its monolayer (phosphorene) and few-layers in field-effect transistors has attracted a lot of attention to this elemental two-dimensional material. Various studies on optimization of black phosphorus field-effect transistors, PN junctions, photodetectors, and other applications have been demonstrated. Although chemical sensing based on black phosphorus devices was theoretically predicted, there is still no experimental verification of such an important study of this material. In this article, we report on chemical sensing of nitrogen dioxide (NO_2) using field-effect transistors based on multilayer black phosphorus. Black phosphorus sensors exhibited increased conduction upon NO_2 exposure and excellent sensitivity for detection of NO_2 down to 5 ppb. Moreover, when the multilayer black phosphorus field-effect transistor was exposed to NO_2 concentrations of 5, 10, 20, and 40 ppb, its relative conduction change followed the Langmuir isotherm for molecules adsorbed on a surface. Additionally, on the basis of an exponential conductance change, the rate constants for adsorption and desorption of NO_2 on black phosphorus were extracted for different NO_2 concentrations, and they were in the range of 130−840 s. These results shed light on important electronic and sensing characteristics of black phosphorus, which can be utilized in future studies and applications.

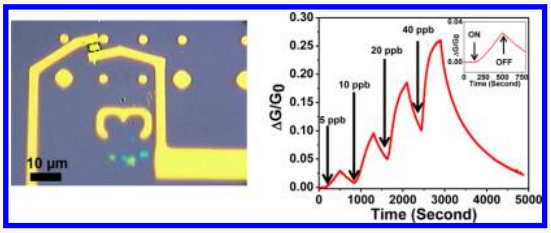

KEYWORDS: black phosphorus · phosphorene · chemical sensing · gas sensing · NO_2 · charge transfer

Recently, the rediscovery of black phosphorus (BP)[1−3] as a new single-element two-dimensional (2D) layered material has sparked the interest of scientists in various fields. Electronic and optical properties showed great promise for using BP in numerous applications. The field-effect transistor (FET) of few-layer BP exhibited high charge mobility, anisotropic transport behavior, high operating frequencies, and relatively high current on/off ratios, making BP a potential candidate for future electronics.[1−6] The recently reported device optimization techniques of BP FETs have yielded transistors with even better performance (*e.g.*, higher mobility and lower contact resistance).[7−10] In addition, optical applications including photovoltaics (PV), photodetectors, and imaging devices were created using BP FETs with different device structures.[9,11−14] Moreover, passivation and stability of black phosphorus has also been studied.[15,16] On the other hand, other applications such as chemical sensing of BP remain only theoretically explored.[17]

Chemical sensing using various nanomaterials is one of the most promising applications, due to the inherent large surface-to-volume ratios. A variety of nanomaterials including carbon nanotubes,[18,19] nanowires,[20,21] and graphene[22,23] were extensively studied for chemical and gas sensing applications. In the 2D family, both exfoliated and chemical-vapor-deposited (CVD) MoS_2 with various thicknesses were used for chemical sensing. The sensitivity of these sensors varied significantly depending on flake thickness, metal contacts, method of synthesis, and other factors.[24−28] For example, chemical sensitivity of MoS_2 FETs to nitrogen dioxide (NO_2) varied from a few hundred parts per million (ppm) in exfoliated samples to a few parts per billion (ppb) in monolayer CVD samples.[26,28]

NO_2 is a common gas produced as a byproduct in industrial plants and vehicles. This gas is hazardous to humans and can cause a number of health problems. According to the U.S. Department of Environmental Protection Agency (EPA), exposure to NO_2 concentrations larger than 53 ppb can cause possible health problems.[29] Consequently, detection of this gas with sensitivities better than the aforementioned limit is of extreme importance. BP, being a 2D material, is predicted to be sensitive to

* Address correspondence to chongwuz@usc.edu.

Received for review April 1, 2015 and accepted May 4, 2015.

Published online 10.1021/acsnano.5b01961

various chemicals with comparable or better sensitivities than MoS_2 and graphene because the adsorption energies of molecules such as NO_2 and NO are larger with BP than with graphene and MoS_2.[17] On the basis of our knowledge, there is yet no systematic experimental verification of gas and/or chemical sensing of BP FETs.

In this report, we investigated the chemical sensing performance of multilayer BP FET to NO_2 gas. We studied the stability of our BP sensors by Raman spectroscopy of flakes before and after sensing, which revealed no difference in the spectra, indicating the multilayer BP was stable for the time frame, and repeated sensing we used. In our experiment, we exposed the BP FET to varying concentrations of NO_2 and monitored the relative conductance change in the device. The BP FET showed a systematic increase in conductance with varying concentrations, indicative of hole doping charge transfer caused by NO_2 molecules. The multilayer BP sensor exhibited a clear conductance change to NO_2 concentrations as low as 5 ppb comparing favorably with the performance of almost all other 2D sensors including monolayer MoS_2.[26,28] Moreover, the devices showed a good recovery to the original conductance after flushing the device with argon, suggesting a reversible adsorption and desorption of NO_2. The relative conductance change fitted fairly well with Langmuir Isotherm for molecular adsorption on a surface. This implies that NO_2 molecular adsorption *via* site binding and charge transfer are the sensing mechanisms for our BP devices. Additionally, we studied the adsorption and desorption rates of NO_2 molecules on the BP surface and derived the rate constants for various NO_2 concentrations. We also examined the drain current *vs* drain voltage (I_d-V_d) and drain current *vs* gate voltage (I_d-V_g) of the BP FET under varying concentrations of NO_2, which showed a systematic increase in conductance and good consistency with Langmuir Isotherm. The results presented in this paper may stimulate further study on the interaction between 2D materials and gas molecules, and may lead to various sensing applications.

RESULTS AND DISCUSSIONS

Figure 1a shows a schematic of the BP device used in this study. First, chemically synthesized BP flakes (see Methods) were exfoliated, using a scotch tape, on a P^{2+} Si/300 nm SiO_2 substrate and subsequently patterned with contact metals (0.5 nm Ti/50 nm Au) as source and drain electrodes. In the back gate configuration, the P^{2+} Si acts as a back gate and the 300 nm SiO_2 is the dielectric. Figure 1b reveals an optical image showing the multilayer BP FET used for NO_2 sensing. The I_d-V_d curves of the device at different back gate voltages and an inset of an I_d-V_g curve are shown in Figure 1c. The linearity of I_d-V_d curves suggests Ohmic contacts between Au and multilayer BP. The nondepletable performance of the multilayer BP flake is due to the electric field screening effect in thick BP flakes.[1−3] Figure 1d shows an atomic force microscope (AFM) image of the multilayer BP sensor and a height profile revealing a thickness of ~55 nm. The use of thick BP flakes is of extreme importance to the stability of the sensor and it was recently applied to other applications of BP such as imaging.[11] Generally, a stable performance over the sensing experiment is required for reliable sensing. Specifically, BP FETs, using relatively thin BP, have displayed degradation in performance under ambient conditions due to the oxidation of phosphorus. Recently, several solutions were developed to encapsulate and passivate BP FETs to maintain good performance under ambient conditions.[15,30,31] These methods are not applicable for sensing applications since direct exposure of the device active material to the chemical is required. Accordingly, we decided to use thick BP flakes for our sensing experiments to enhance the stability of the device and reduce degradation under exposure to NO_2. Although thinner BP flakes may theoretically offer better sensing performance because of the larger surface-to-volume ratio and larger bandgaps (*i.e.*, reduced charge density), thinner flakes maybe more affected by oxidation than thicker flakes. On the basis of our experiments, we observed that continuous electrical measurements of thin BP flakes in air made the BP FET fail (Supporting Information Figure S1). On the other hand, a bias stress test of a thick BP flake in air showed relatively stable performance with a conductance variation less than 4% (Figure 1e). To isolate the effect of NO_2 on BP from other species such as oxygen and water vapor, we carried out the sensing experiments in an argon environment (*i.e.*, NO_2 diluted in argon). Nonetheless, the relatively stable conductance value in air is promising for more practical future sensing applications. To further investigate the effect of NO_2 exposure on BP flakes we compared the Raman spectrum of BP flakes before and after exposure to NO_2. Due to the anisotropic nature of BP, care was taken to keep the laser polarization, for a specific flake, in the same direction in all Raman measurements. Figure 1f shows a Raman spectroscopy taken on a multilayer BP flake before and after exposure to 800 ppb NO_2 for ~30 min. It can be seen that all peaks associated with BP (A^1_g at ~362 cm^{-1}, A^2_g at ~466 cm^{-1}, and B_{2g} at ~440 cm^{-1}) remain in the same positions and show similar relative peak intensity ratios before and after exposure. This suggests minimal chemical degradation of multilayer BP flakes used in our experiments during NO_2 exposure.

The NO_2 sensing experiment starts by loading the device in a gas chamber while flushing the system with argon for 10 min. Afterward, the NO_2 gas is diluted with argon to produce various concentrations and

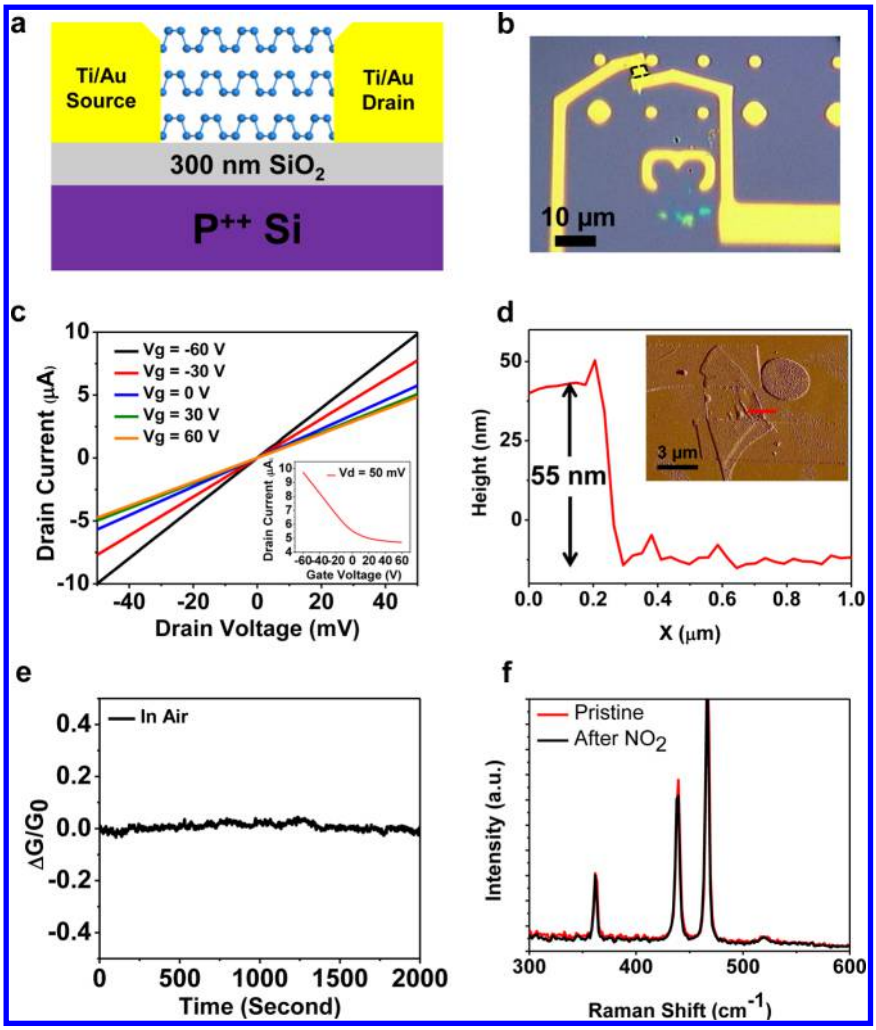

Figure 1. Schematic, images, electronic properties and stability of multilayer BP FET used for chemical sensing. (a) Scheme of a multilayer BP FET. (b) An optical image of the multilayer BP flake between two Ti/Au electrodes used in this study. The BP flake is bordered by a dashed black line to guide the eye. (c) I_d-V_d curves of the multilayer BP FET in (b) showing linear curves, which is a characteristic of an ohmic contacted device. Inset shows an I_d-V_g curve measured at 50 mV V_d with a nondepletable current. (d) An AFM height profile of the BP flake revealing a height of 55 nm. Inset showing an AFM amplitude image of the multilayer BP FET in (b). (e) A bias stress test of a BP multilayer flake in air showing a maximum fluctuation in relative conductance of less than 4%. (f) Raman spectra of multilayer BP FET before (red) and after (black) exposure to 800 ppb NO_2 for 30 min showing qualitatively identical spectra (A^1_g at ~362 cm^{-1}, A^2_g at ~466 cm^{-1} and B_{2g} at ~440 cm^{-1}).

the BP device is subsequently exposed to the desired concentration. After the exposure to a certain NO_2 concentration, the system is flushed with argon for 300 s to partially recover the device and to observe a conductance change opposite to the NO_2 exposure period. Finally, when the device is exposed to all desired concentrations, the system is flushed with argon until the device recovers to the original conductance value. Figure 2 shows the results from the above-described sensing experiment. In Figure 2a, the relative conductance change $\Delta G/G_0$ is plotted *vs* time (where $\Delta G = G - G_0$, G is the instantaneous conductance of the device, and G_0 is the conductance of the device before exposure to NO_2). The inset of Figure 2a illustrates the point in time where the device is exposed to 5 ppb NO_2 concentration (*i.e.*, ON) and when the device is flushed with argon (*i.e.*, OFF). It can be clearly observed that the BP sensor responds to NO_2 concentrations down to 5 ppb evident by a conductance change of 2.9%. The relatively high sensitivity to NO_2 for multilayer BP is very interesting and may be further improved by reducing the layer number and increasing the surface-to-volume ratio. Additionally, it can be seen that the conductance change is monotonic and systematically increases as the concentration increases from 5 to 40 ppb. After exposure to all NO_2 concentrations, the device recovers while being flushed with argon in a period of ~35 min and can be used again for another round of sensing (Figure 2a). In Figure 2b, the measured $\Delta G/G_0$ is plotted *vs* NO_2 gas concentration. $\Delta G/G_0$ is extracted by taking the difference of the ON and OFF values (Figure 2a inset) for each concentration. The data points in Figure 2b fit with Langmuir Isotherm for molecules adsorbed on a

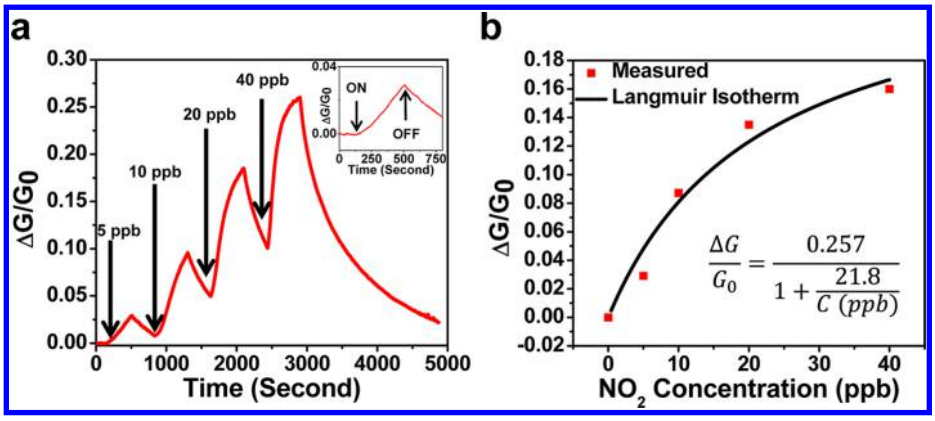

Figure 2. NO_2 gas sensing performance of multilayer BP FET. (a) Relative conductance change ($\Delta G/G_0$) *vs* time in seconds for a multilayer BP sensor showing a sensitivity to NO_2 concentrations (5−40 ppb). Inset shows a zoomed in image of a 5 ppb NO_2 exposure response with identification of points in time where the NO_2 gas is switched on and off. (b) $\Delta G/G_0$ plotted *vs* NO_2 concentration applied to the BP FET showing an agreement between the measured values (red squares) and the fitted Langmuir isotherm. The equation in the bottom right is the fitted Langmuir isotherm.

surface with equation:

$$\frac{\Delta G}{G_0} = \frac{0.257}{1+\frac{21.8}{C\ (\text{ppb})}}$$

(where C is the concentration in ppb). The fitting further confirms that charge transfer is the sensing mechanism for NO_2 sensing in the multilayer BP devices. Moreover, repeated sensing experiments revealed very similar sensing performances of the same device suggesting a stable performance over the time frame of our experiment (Supporting Information Figure S3). We note that the BP sensor is not specifically selective to NO_2. To improve the selectivity of the BP sensor to NO_2, further efforts must be applied to modify the BP surface or sensor structure to be selective to a specific chemical species.

We define the sensor response time as the time required to change the conductance after introducing either NO_2 (conductance increase) or argon (conductance decrease) in a specific range by 90%. Accordingly, we calculated the response time of our sensor to be in the range of ∼280−350 s for different concentrations. This value is an indication of the rate the molecules are adsorbed on BP surface and it is comparable to other reports using other 2D materials, such as MoS_2 as gas sensors.[24,26,28] To further analyze the adsorption and desorption of NO_2 molecules on BP, we extracted the absorption/desorption rate constants (τ) of the multilayer BP device. The first-order rate equation is of the form: $G = G_f + (G_0 - G_f)e^{-t/\tau}$, where G is the instantaneous conductance, G_f is the final conductance after the end of an adsorption/desorption period, G_0 is the initial conductance before an adsorption/desorption period, and t is the time.[32] Figure 3a, shows the measured conductance decrease associated with NO_2 desorption and the fitted curve when the BP FET is flushed with argon after being in a 20 ppb NO_2 environment. The measured and fitted curves show a

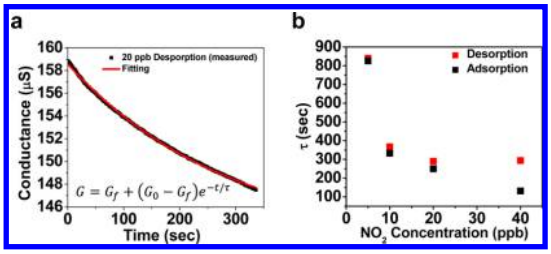

Figure 3. NO_2 gas sensing adsorption and desorption rate study. (a) Measured time-dependent conductance change of a multilayer BP FET (black) flushed with argon after being exposed to 20 ppb NO_2, showing a continuous decrease in conductance and the corresponding fitted curve (red) using the equation in the bottom of (a). (b) Rate constant (τ) extracted from curve fitting *vs* NO_2 concentration showing a saturation behavior for higher concentrations of NO_2.

nearly perfect agreement with a fitting error of ∼1.5%. This agreement suggests that there is only one time constant and therefore only one mechanism associated with NO_2 molecular adsorption/desorption in our experiment. Theoretical study of NO_2 preferential binding position and binding energy was previously reported.[17] The single mechanism of adsorption/desorption corresponds to a single binding energy, which is most likely the preferential binding position that corresponds to a distance of 2.2 Å between NO_2 and phosphorus atoms with no covalent bond formation.[17] Figure 3b plots the adsorption and desorption rate constants (τ) *vs* different concentrations of NO_2. The extracted τ values varied from ∼130 s for a concentration of 5 ppb to ∼840 s for a concentration of 40 ppb. It can be observed that τ, which is a metric for how fast the NO_2 adsorption/desorption process is, decreases as the gas concentration increases and saturates at high concentrations.

The surprisingly high sensitivity of the thick (*i.e.*, 55 nm) multilayer BP flake compared to other multilayer 2D materials such as MoS_2 is worth noting.[25,26] For instance, He *et al.* observed a ∼1% change in $\Delta G/G_0$ when exposing an 18 nm MoS_2 flake to 1200 ppb NO_2, while we observe a 2.9% change in $\Delta G/G_0$ when

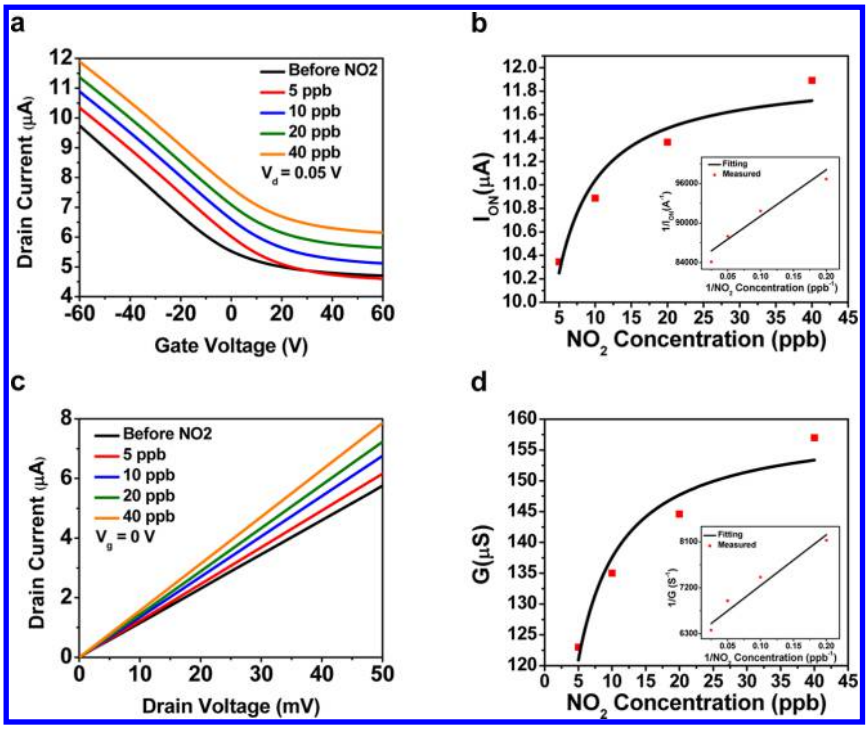

Figure 4. Electronic properties of multilayer BP FET under different NO_2 gas concentrations. (a) I_d-V_g curves of multilayer BP FET under different concentrations of NO_2 showing a clear upshift in the curves as the concentrations increase. (b) Measured I_{ON} *vs* NO_2 concentration (red) and the corresponding fitted Langmuir isotherm (black) showing a good agreement. Inset shows $1/I_{ON}$ vs $1/NO_2$ concentration exhibiting a linear relation further illustrating Langmuir isotherm fitting. (c) I_d-V_d curves of the same device under different NO_2 concentrations showing a monotonic increase in conductance with increasing NO_2 concentrations. (d) Measured G *vs* NO_2 concentration (red) and the corresponding fitted Langmuir isotherm (black) showing good agreement. Inset shows $1/G$ *vs* $1/NO_2$ concentration exhibiting a linear relation.

exposing a 55 nm BP flake to 5 ppb NO_2 (240 times lower in concentration).[25] This staggering difference in response of multilayer samples is potentially material dependent. As we mentioned earlier, the high adsorption energies of NO_2 to BP is one reason causing the high sensitivity of our BP gas sensors.[17] Additionally, it was theoretically predicted and experimentally observed that BP layers have less out-of-plane conductance than other 2D materials such as graphene and MoS_2.[33−35] This low conductance in the out-of-plane direction in BP compared to the in-plane conductance may explain the high sensitivity we observe. Since only the topmost BP layer and edges are exposed to NO_2 during sensing, and since the metal contact to the multilayer BP flake is mostly to the top layer, the transport and doping of the top layers may dominantly control the conductance of the device because of the low conductance in the out-of-plane direction. To further explore the conductance of the out-of-plane direction in BP, we fabricated a vertical structure comprised of a monolayer graphene bottom contact to multilayer BP and a 0.5 nm Ti/50 nm Au top contact (Supporting Information Figure S2). It can be observed that the ON current value in the vertical BP transistor structure (Supporting Information Figure S2) is approximately 2 orders of magnitude lower than that in the traditional lateral transport FET structure (*i.e.*, 10 μA for V_d = 0.05 V in lateral FET compared to 20−100 nA for V_d = 0.1 V in vertical FET). Moreover, comparing to a vertical MoS_2 with flake thicknesses in the same range and similar device structure, BP vertical FET structure revealed a vertical current density of 0.5−2.4 A/cm^2 at V_d = 0.2 V (Supporting Information Figure S2), while MoS_2 at the same V_d exhibited a current density of ~800 A/cm^2.[36] This notably large difference further supports our explanation and hypothesis about the observed high sensitivity in multilayer BP sensors compared to its other 2D counterparts.

We further characterize the electronic properties of the multilayer BP FET *via* observing the change in I_d-V_d and I_d-V_g curves after exposing the device to different concentrations. First, the device was flushed with argon to clear the system from any contaminants or residual gas species. Then the device was exposed to a specific NO_2 concentration for 500 s. Subsequently, measurements of I_d-V_d and I_d-V_g curves were recorded while the device is still exposed to NO_2. Afterward, the device was flushed with argon for 300 s before exposing the device to a new concentration of NO_2. The time of 500 s we used to expose BP to NO_2, and the time of 300 s we used to flush the BP devices for recovery are chosen as reasonable durations for typical chemical sensing and recovery experiments. As we can tell from the response amplitudes and speeds in Figure 2a, either shorter or longer exposure times can also be used. Figure 4a shows the I_d-V_g curves of

the BP device under different concentrations. An upshift in the curves with increasing NO_2 concentrations associated with extra hole doping was observed. Figure 4b plots the on current (I_{ON}) (defined as current at $V_g = -60$ V) extracted from Figure 4a *vs* the concentration of NO_2 to which the BP device was exposed. The measured data points reveal a saturation behavior at higher concentrations and follow the Langmuir Isotherm with equation:

$$I_{ON} = \frac{1.19 \times 10^{-5}}{1 + \frac{0.836}{C\ (\text{ppb})}}\ (A)$$

which further supports that charge transfer is the main mechanism for BP FET sensors. The inset of Figure 4b shows that $1/I_{ON}$ *vs* $1/C$ (ppb) has a linear relationship, which is another representation of the Langmuir Isotherm in Figure 4b. I_d-V_d curves at different concentrations of NO_2 are plotted in Figure 4c. As can be seen, the conductance increases monotonically with increasing NO_2 concentrations. Moreover, the I_d-V_d curves maintain their linearity with various NO_2 concentrations indicating minimal effect of Schottky barrier modulation induced by NO_2 exposure under the conditions we used in the experiment. Figure 4d shows the conductance (G) of our BP sensor extracted from Figure 4c *vs* the concentration of NO_2. The fitted Langmuir Isotherm equation is

$$G = \frac{1.6 \times 10^{-4}}{1 + \frac{1.59}{C\ (\text{ppb})}}\ (S)$$

which agrees with the measured data points. Similar to Figure 4b, the inset of Figure 4d shows a linear dependence of $1/G$ *vs* $1/C$ (ppb) which agrees with the Langmuir Isotherm fitting.

CONCLUSIONS

In summary, we experimentally demonstrated NO_2 gas sensing performance of multilayer BP FETs. The BP sensors were sensitive to NO_2 concentration down to 5 ppb making them comparable in sensitivity to the best 2D material based sensors. Raman spectroscopy comparison revealed no apparent change in the spectra before and after exposure to NO_2, which shows that thick BP flakes can maintain their relative stability after sensing. Moreover, the BP device sensing performance fitted well with the Langmuir Isotherm for molecules adsorbed on a surface, which confirms charge transfer as the dominant mechanism for sensing. The systematic increase in conductance with increasing NO_2 concentrations suggests NO_2 molecules withdraw electrons and dope BP flakes with holes. These results lay the groundwork for BP to be applied to various sensing applications including chemical, gas, and biosensors.

METHODS

BP Synthesis. We synthesized BP samples from red phosphorus (Chempur, 99.999+ %) and tin/tin(IV) iodide (Sn/SnI_4 = 10/5 mg per 250 mg batch) in evacuated ($p < 10^{-3}$ mbar) silica ampules according to literature procedures.[37] Subsequently, the temperature of the starting materials was raised to 650 °C in a period of 8 h and that temperature was held for 5 h. Then, the oven chamber was cooled down to 550 °C in a period of 7.5 h and was kept at that temperature for 6 h. Eventually, the mixture was cooled to room temperature.

BP Device Fabrication. BP flakes were exfoliated using a commercial tape on a P^{2+} Si/300 nm SiO_2 substrate with alignment marks patterned. After the flakes were located using optical microscopy, electron beam lithography (EBL) defined electrodes were patterned on the target BP flake. Subsequently, electron beam evaporation of 0.5 nm Ti as an adhesion layer and then 50 nm thick Au layer for contacts were carried out. Then, the sample was soaked in acetone for ~30 min to do metal lift-off. Afterward, the devices were manually bonded using indium wire bonds after mounting the substrate on a chip carrier. Finally, devices were loaded inside the gas sensing chamber and measurements were recorded.

NO_2 Gas Sensing. Gas sensing was carried out by exposing the BP FET device to NO_2 gas diluted in argon in a closed chamber. Concentrations of NO_2 were adjusted by changing the flow rates of both gases while keeping the total flow rate constant. For each curve, the device was exposed to the desired concentration for 500 s and then flushed with argon for 300 s. Similar procedure was followed to measure I_d-V_d and I_d-V_g for BP devices.

Conflict of Interest: The authors declare no competing financial interest.

Supporting Information Available: Failure of a BP thin flake device in air (Figure S1), BP vertical FET measurements (Figure S2), and repeatability of BP sensor (Figure S3). The Supporting Information is available free of charge on the ACS Publications website at DOI: 10.1021/acsnano.5b01961.

REFERENCES AND NOTES

1. Li, L.; Yu, Y.; Ye, G. J.; Ge, Q.; Ou, X.; Wu, H.; Feng, D.; Chen, X. H.; Zhang, Y. Black Phosphorus Field-Effect Transistors. *Nat. Nanotechnol.* **2014**, *9*, 372–377.
2. Xia, F.; Wang, H.; Jia, Y. Rediscovering Black Phosphorus as an Anisotropic Layered Material For Optoelectronics and Electronics. *Nat. Commun.* **2014**, *5*, No. 4458.
3. Liu, H.; Neal, A. T.; Zhu, Z.; Luo, Z.; Xu, X.; Tománek, D.; Ye, P. D. Phosphorene: An Unexplored 2D Semiconductor with a High Hole Mobility. *ACS Nano* **2014**, *8*, 4033–4041.
4. Koenig, S. P.; Doganov, R. A.; Schmidt, H.; Castro Neto, A. H.; Özyilmaz, B. Electric Field Effect in Ultrathin Black Phosphorus. *Appl. Phys. Lett.* **2014**, *104*, 103106.
5. Wang, H.; Wang, X.; Xia, F.; Wang, L.; Jiang, H.; Xia, Q.; Chin, M. L.; Dubey, M.; Han, S.-j. Black Phosphorus Radio-Frequency Transistors. *Nano Lett.* **2014**, *14*, 6424–6429.
6. Zhang, X.; Xie, H.; Liu, Z.; Tan, C.; Luo, Z.; Li, H.; Lin, J.; Sun, L.; Chen, W.; Xu, Z. Black Phosphorus Quantum Dots. *Angew. Chem., Int. Ed.* **2015**, *54*, 3653–3657.
7. Kamalakar, M. V.; Madhushankar, B. N.; Dankert, A.; Dash, S. P. Low Schottky Barrier Black Phosphorus Field-Effect Devices with Ferromagnetic Tunnel Contacts. *Small*, DOI: 10.1002/smll.201402900.
8. Li, L.; Ye, G. J.; Tran, V.; Fei, R.; Chen, G.; Wang, H.; Wang, J.; Watanabe, K.; Taniguchi, T.; Yang, L. et al. Quantum

Oscillations in Black Phosphorus Two-Dimensional Electron Gas. *arXiv* **2014**, arXiv:1411.6572.
9. Buscema, M.; Groenendijk, D. J.; Steele, G. A.; van der Zant, H. S. J.; Castellanos-Gomez, A., Photovoltaic Effect in Few-Layer Black Phosphorus PN Junctions Defined by Local Electrostatic Gating. *Nat. Commun.* **2014**, *5*.
10. Du, Y.; Liu, H.; Deng, Y.; Ye, P. D. Device Perspective for Black Phosphorus Field-Effect Transistors: Contact Resistance, Ambipolar Behavior, and Scaling. *ACS Nano* **2014**, *8* (10), 10035–10042.
11. Engel, M.; Steiner, M.; Avouris, P. Black Phosphorus Photodetector for Multispectral, High-Resolution Imaging. *Nano Lett.* **2014**, *14*, 6414–6417.
12. Buscema, M.; Groenendijk, D. J.; Blanter, S. I.; Steele, G. A.; van der Zant, H. S. J.; Castellanos-Gomez, A. Fast and Broadband Photoresponse of Few-Layer Black Phosphorus Field-Effect Transistors. *Nano Lett.* **2014**, *14*, 3347–3352.
13. Youngblood, N.; Chen, C.; Koester, S. J.; Li, M. Waveguide-Integrated Black Phosphorus Photodetector with High Responsivity and Low Dark Current. *Nat. Photonics* **2015**, 10.1038/nphoton.2015.23.
14. Yuan, H.; Liu, X.; Afshinmanesh, F.; Li, W.; Xu, G.; Sun, J.; Lian, B.; Ye, G.; Hikita, Y.; Shen, Z. et al. Broadband Linear-Dichroic Photodetector in a Black Phosphorus Vertical p-n Junction. *arXiv* **2014**, arXiv:1409.4729.
15. Wood, J. D.; Wells, S. A.; Jariwala, D.; Chen, K.-S.; Cho, E.; Sangwan, V. K.; Liu, X.; Lauhon, L. J.; Marks, T. J.; Hersam, M. C. Effective Passivation of Exfoliated Black Phosphorus Transistors against Ambient Degradation. *Nano Lett.* **2014**, *14*, 6964–6970.
16. Ziletti, A.; Carvalho, A.; Campbell, D. K.; Coker, D. F.; Castro Neto, A. H. Oxygen Defects in Phosphorene. *Phys. Rev. Lett.* **2015**, *114*, 046801.
17. Kou, L.; Frauenheim, T.; Chen, C. Phosphorene as a Superior Gas Sensor: Selective Adsorption and Distinct I-V Response. *J. Phys. Chem. Lett.* **2014**, *5*, 2675–2681.
18. Kong, J.; Franklin, N. R.; Zhou, C.; Chapline, M. G.; Peng, S.; Cho, K.; Dai, H. Nanotube Molecular Wires as Chemical Sensors. *Science* **2000**, *287*, 622–625.
19. Qi, P.; Vermesh, O.; Grecu, M.; Javey, A.; Wang, Q.; Dai, H.; Peng, S.; Cho, K. J. Toward Large Arrays of Multiplex Functionalized Carbon Nanotube Sensors for Highly Sensitive and Selective Molecular Detection. *Nano Lett.* **2003**, *3*, 347–351.
20. Zhang, D.; Liu, Z.; Li, C.; Tang, T.; Liu, X.; Han, S.; Lei, B.; Zhou, C. Detection of NO_2 Down to ppb Levels Using Individual and Multiple In_2O_3 Nanowire Devices. *Nano Lett.* **2004**, *4*, 1919–1924.
21. Zou, X.; Wang, J.; Liu, X.; Wang, C.; Jiang, Y.; Wang, Y.; Xiao, X.; Ho, J. C.; Li, J.; Jiang, C.; et al. Rational Design of Sub-Parts per Million Specific Gas Sensors Array Based on Metal Nanoparticles Decorated Nanowire Enhancement-Mode Transistors. *Nano Lett.* **2013**, *13*, 3287–3292.
22. Schedin, F.; Geim, A. K.; Morozov, S. V.; Hill, E. W.; Blake, P.; Katsnelson, M. I.; Novoselov, K. S. Detection of Individual Gas Molecules Adsorbed on Graphene. *Nat. Mater.* **2007**, *6*, 652–655.
23. Abbas, A. N.; Liu, G.; Liu, B.; Zhang, L.; Liu, H.; Ohlberg, D.; Wu, W.; Zhou, C. Patterning, Characterization, and Chemical Sensing Applications of Graphene Nanoribbon Arrays Down to 5 nm Using Helium Ion Beam Lithography. *ACS Nano* **2014**, *8*, 1538–1546.
24. Li, H.; Yin, Z.; He, Q.; Li, H.; Huang, X.; Lu, G.; Fam, D. W. H.; Tok, A. I. Y.; Zhang, Q.; Zhang, H. Fabrication of Single- and Multilayer MoS_2 Film-Based Field-Effect Transistors for Sensing NO at Room Temperature. *Small* **2012**, *8*, 63–67.
25. He, Q.; Zeng, Z.; Yin, Z.; Li, H.; Wu, S.; Huang, X.; Zhang, H. Fabrication of Flexible MoS_2 Thin-Film Transistor Arrays for Practical Gas-Sensing Applications. *Small* **2012**, *8*, 2994–2999.
26. Late, D. J.; Huang, Y.-K.; Liu, B.; Acharya, J.; Shirodkar, S. N.; Luo, J.; Yan, A.; Charles, D.; Waghmare, U. V.; Dravid, V. P.; et al. Sensing Behavior of Atomically Thin-Layered MoS_2 Transistors. *ACS Nano* **2013**, *7*, 4879–4891.
27. Perkins, F. K.; Friedman, A. L.; Cobas, E.; Campbell, P. M.; Jernigan, G. G.; Jonker, B. T. Chemical Vapor Sensing with Monolayer MoS_2. *Nano Lett.* **2013**, *13*, 668–673.
28. Liu, B.; Chen, L.; Liu, G.; Abbas, A. N.; Fathi, M.; Zhou, C. High-Performance Chemical Sensing Using Schottky-Contacted Chemical Vapor Deposition Grown Monolayer MoS_2 Transistors. *ACS Nano* **2014**, *8*, 5304–5314.
29. U.S. Department of Environmental Protection Agency. http://www.epa.gov/airquality/nitrogenoxides/.
30. Xi, L.; Rahbarihagh, Y.; Hwang, J. C. M.; Han, L.; Yuchen, D.; Ye, P. D. Temporal and Thermal Stability of Al_2O_3-Passivated Phosphorene MOSFETs. *IEEE Electron Device Lett.* **2014**, *35*, 1314–1316.
31. Doganov, R. A.; O'Farrell, E. C. T.; Koenig, S. P.; Yeo, Y.; Ziletti, A.; Carvalho, A.; Campbell, D. K.; Coker, D. F.; Watanabe, K.; Taniguchi, T. et al. Accessing the Transport Properties of Pristine Few-Layer Black Phosphorus by van der Waals Passivation in Inert Atmosphere. *arXiv* **2014**, arXiv:1412.1274.
32. Zhang, Y.; Kolmakov, A.; Chretien, S.; Metiu, H.; Moskovits, M. Control of Catalytic Reactions at the Surface of a Metal Oxide Nanowire by Manipulating Electron Density Inside It. *Nano Lett.* **2004**, *4*, 403–407.
33. Low, T.; Rodin, A. S.; Carvalho, A.; Jiang, Y.; Wang, H.; Xia, F.; Castro Neto, A. H. Tunable Optical Properties of Multilayer Black Phosphorus Thin Films. *Phys. Rev. B* **2014**, *90*, 075434.
34. Takahashi, T.; Gunasekara, N.; Ohsawa, H.; Ishii, H.; Kinoshita, T.; Suzuki, S.; Sagawa, T.; Kato, H.; Miyahara, T.; Shirotani, I. Angle-Resolved Photoemission Study of Black Phosphorus: Interlayer Energy Dispersion. *Phys. Rev. B* **1986**, *33*, 4324–4326.
35. Han, C. Q.; Yao, M. Y.; Bai, X. X.; Miao, L.; Zhu, F.; Guan, D. D.; Wang, S.; Gao, C. L.; Liu, C.; Qian, D.; et al. Electronic Structure of Black Phosphorus Studied by Angle-Resolved Photoemission Spectroscopy. *Phys. Rev. B* **2014**, *90*, 085101.
36. Yu, W. J.; Li, Z.; Zhou, H.; Chen, Y.; Wang, Y.; Huang, Y.; Duan, X. Vertically Stacked Multi-Heterostructures of Layered Materials for Logic Transistors and Complementary Inverters. *Nat. Mater.* **2012**, *12*, 246–252.
37. Köpf, M.; Eckstein, N.; Pfister, D.; Grotz, C.; Krüger, I.; Greiwe, M.; Hansen, T.; Kohlmann, H.; Nilges, T. Access and *in Situ* Growth of Phosphorene-Precursor Black Phosphorus. *J. Cryst. Growth* **2014**, *405*, 6–8.